Selective Hydrogenation of Furfural Acetone over a Cu Catalyst: Combined Theoretical and Experimental Study

Michael Rebarchik[†,a], Evangelos Smith[†,a], Hochan Chang[a], James A. Dumesic[a], and Manos Mavrikakis[a]*

[a]*Department of Chemical and Biological Engineering, University of Wisconsin–Madison, 1415 Engineering Drive, Madison, Wisconsin 53706, United States*

[†] M.R. and E.S. contributed equally

*** Corresponding Author:**

Manos Mavrikakis (emavrikakis@wisc.edu, ORCID 0000-0002-5293-5356)

Abstract

The selective hydrogenation of biomass-derived hydroxymethyl furfural (HMF)-acetone-HMF (HAH) presents an alternative route to producing highly functionalized polyesters and polyurethanes. While HAH undergoes furan ring hydrogenation over Pd, Ru, and Ni catalysts, furan ring hydrogenation is not observed over Cu. Herein, we combine reaction kinetics experiments and density functional theory calculations to elucidate the selective hydrogenation behavior of HAH over Cu catalysts. We identified furfural acetone (FAc) as a suitable surrogate for modeling HAH hydrogenation over Cu surfaces and performed reaction kinetics experiments between temperatures of 313-393 K and a H_2 partial pressure of 30 bar FAc. Similar to the behavior of HAH, hydrogenation of FAc follows a consecutive 2-step hydrogenation pathway over Cu and does not undergo furan ring hydrogenation. The apparent activation energy barriers for hydrogenation of the aliphatic double bond (0.58 eV) and carbonyl (0.43 eV) of FAc measured in a continuous flow reactor setup are consistent with those reported in prior studies for batch HAH hydrogenation. Reaction orders with respect to each reactant, including H_2 and FAc, were determined to be nearly one. Density functional theory (DFT; GGA-PBE-D3) calculations on Cu(111) showed that the hydrogenation of the aliphatic double bond of FAc is more facile than the hydrogenation of the furan ring, which displays weak interactions with the Cu surface. We determined an apparent activation energy barrier for FAc hydrogenation (0.58 eV) that agreed with our DFT predictions (highest barrier for FAc hydrogenation of 0.57 eV). Our DFT calculations further show that weak interactions between the furan ring and Cu surface are responsible for the selective hydrogenation behavior.

Keywords: selective hydrogenation, furfural acetone, biomass, copper, density functional theory

TOC Graphic

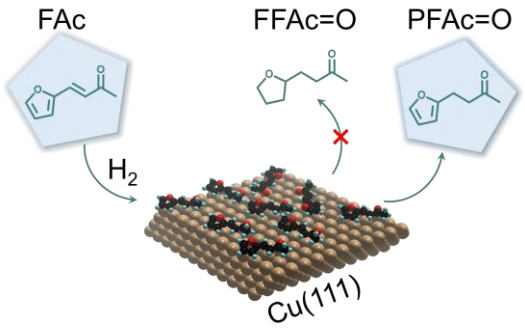

Introduction

Increasing dependence on petroleum-based products has renewed interest in utilizing alternative biomass-derived feedstocks. Among notable biomass-derived chemicals, 5-hydroxymethylfurfural (HMF) has been identified as a versatile platform molecule that can be synthesized sustainably through the selective dehydration of simple sugars.[1–3] Studies have shown that HMF can be obtained in high yields at the laboratory scale, and production can be accomplished using existing chemical infrastructure.[4] It has been demonstrated that HMF and other similar platform molecules can be used to produce higher molecular weight molecules (C_9 - C_{15}) suitable for potential diesel and jet fuels.[5–9] More generally, we recently demonstrated that an HMF-acetone-HMF (HAH) monomer can be obtained in high yields through an aldol condensation.[10] This HAH molecule is a highly functionalized platform chemical that opens pathways for the production of a wide range of C_{15} monomers,[6] organic dyes,[11] and high molecular weight liquid fuels[4] and displays higher stability than HMF.[6] Previous techno-economic analyses have shown that the costs of producing HAH-derived monomers and chemical intermediates derived from HAH are competitive with fossil fuel-based precursors.[12] As a result, HAH, along with its various hydrogenated products, may offer an economically viable, alternative solution to synthesize tunable, functionalized polyurethanes and polyesters.[6] By controlling the degree of hydrogenation, the chemical properties of HAH-derived polymers can be controlled leading to improved thermal stability and stiffness in polymeric products.

In a recent study, we reported the hydrogenation behavior of HAH over various transition metal catalysts.[7] While hydrogenation of the furan ring was reported over Pd and Ru surfaces, Cu surfaces selectively hydrogenated the aliphatic double bonds of HAH, with no further furan ring hydrogenation.[7] In the present paper, we investigate the surface interactions over transition metal catalysts that govern the selective hydrogenation behavior to identify improved catalytic materials. We adopted a combined experimental-theoretical approach to study the selective hydrogenation of HAH over transition metal catalysts. In this approach, we combined detailed reaction kinetics experiments using both batch and continuous flow reactors with first-principles calculations to obtain insights into the surface chemistry occurring on transition metal catalysts.

Given the large molecular size of HAH that would render molecular simulations impractically expensive, we employed a surrogate molecule to model HAH hydrogenation that was more tractable for computational modeling. Through batch reaction kinetic experiments over a Cu/γ-

Al_2O_3 catalyst, we identified furfural acetone (FAc) (shown in Figure 1), which retains all relevant double bonds present in HAH while significantly reducing the molecule size, as a suitable surrogate to describe HAH hydrogenation. Despite lacking the hydroxymethyl group present on the furan ring, the FAc hydrogenation pathway was found to be consistent with that of HAH over a Cu catalyst. Next, we investigated FAc hydrogenation in a continuous flow reactor to extract reaction kinetics parameters. In addition, we performed DFT calculations to model the hydrogenation of FAc over a Cu(111) surface. Using insights from the FAc surrogate, we explored the thermodynamic and structural descriptors that govern HAH hydrogenation over Cu catalysts.

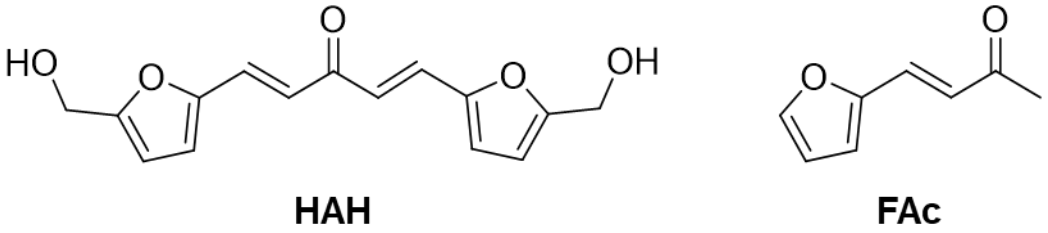

Figure 1. Molecular structures for 5-hydroxymethylfurfural (HMF)-acetone-HMF (HAH) and furfural acetone (FAc), the computational surrogate used as a proxy for HAH.

Through our combined experimental and theoretical investigation, we find that experimental results for selective hydrogenation pathways of FAc are consistent with theoretical predictions over Cu catalysts. We find that a weak interaction between the Cu(111) surface and the furan ring in FAc prohibits furan ring hydrogenation.

Results and Discussion

1 Batch Reaction Experiments

Batch reactor experiments were conducted over a Cu/γ-Al_2O_3 catalyst to compare the hydrogenation behavior of the FAc surrogate with that of HAH. Reaction kinetics experiments were performed using a 45 mL Parr reactor equipped with a dip tube for sampling. The temperature was varied between 313 and 393 K, and a feed solution comprised of 56 mM FAc in 2-propanol was used. For each reaction condition, the concentrations of FAc and hydrogenated products were monitored over time. Structures for all hydrogenated products were confirmed using NMR (Figures S1-S3 in the Supporting Information). The results of these experiments are shown in Figure .

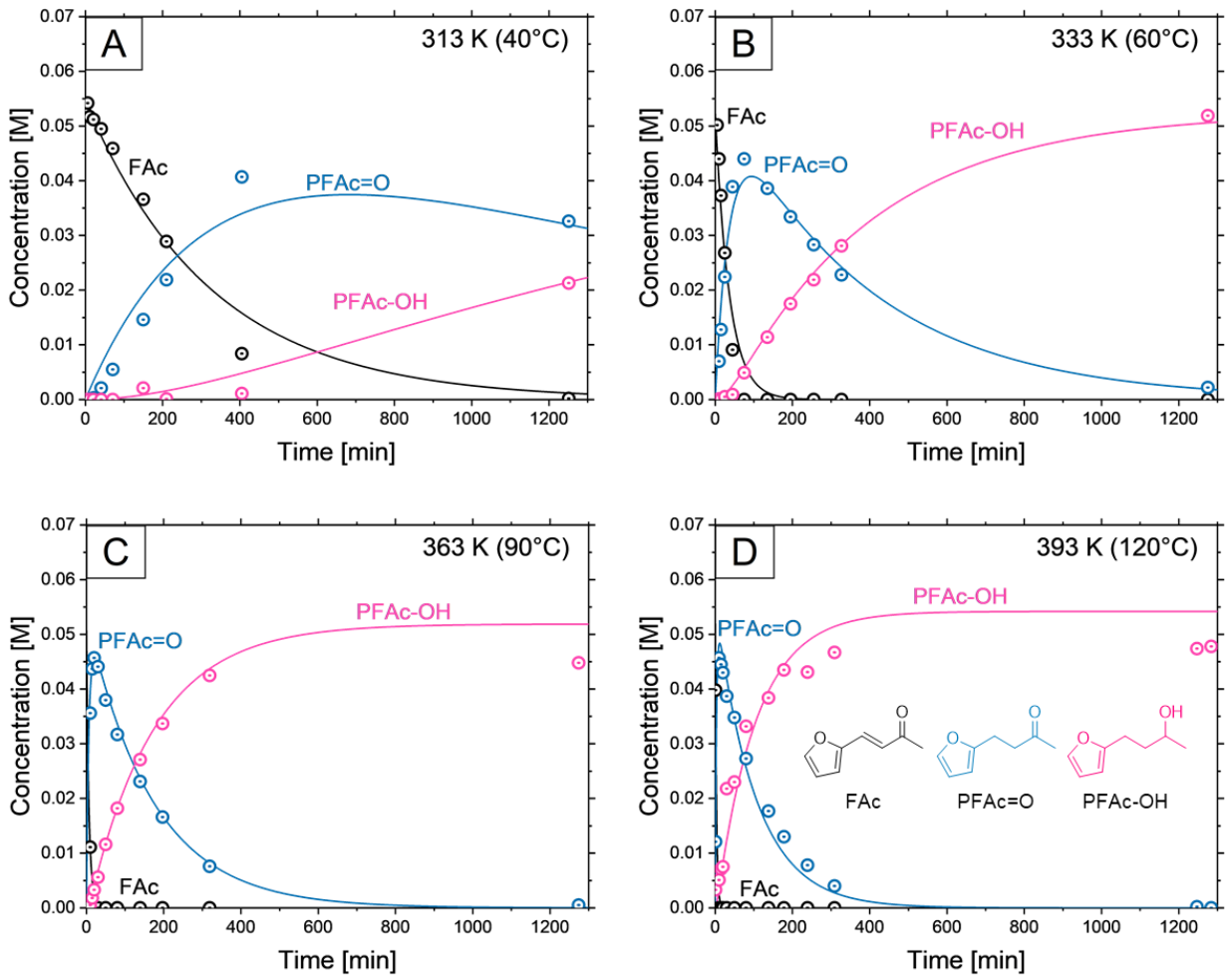

Figure 2. Concentration profiles showing FAc hydrogenation products over a Cu/γ-Al_2O_3 catalyst for A) 313 K, B) 333 K, C) 363 K, and D) 393 K. Circles denote experimental measurements whereas solid lines indicate concentration profiles derived from fitted reaction kinetics parameters. For each experiment, the reactor was loaded with 56 mM FAc dissolved in 30 mL of 2-propanol, pressurized to 30 bar with H_2, and heated to the reaction temperature at a heating rate of 3 K min^{-1}. PFAc stands for partially hydrogenated FAc; Carbonyl and hydroxyl groups in PFAc are abbreviated to =O and -OH, respectively.

From these experiments, FAc was found to proceed through two consecutive hydrogenation events (Figure 2(A)). Using a lumped reaction scheme similar to the 3-step network previously identified for HAH hydrogenation over Cu,[7] the 2-step scheme shown in Scheme 1 was adopted for FAc hydrogenation. In this scheme, FAc is first converted to PFAc=O through the hydrogenation of the aliphatic double bond, followed by cascade hydrogenation of the C=O bond to form PFAc-OH. Notably, the sequence of FAc hydrogenation events was found to be consistent with that of HAH hydrogenation over Cu, and no hydrogenation of the furan rings to fully hydrogenated FAc species (FFAc) was observed. Despite lacking the furan hydroxymethyl group present in HAH, agreement between the hydrogenation pathways of FAc and HAH suggests that

the hydroxymethyl group does not play an active role in the specific surface chemistry. Subsequent DFT calculations also indicate that hydroxyl groups on relevant adsorbed molecules interact weakly with the Cu(111) surface.

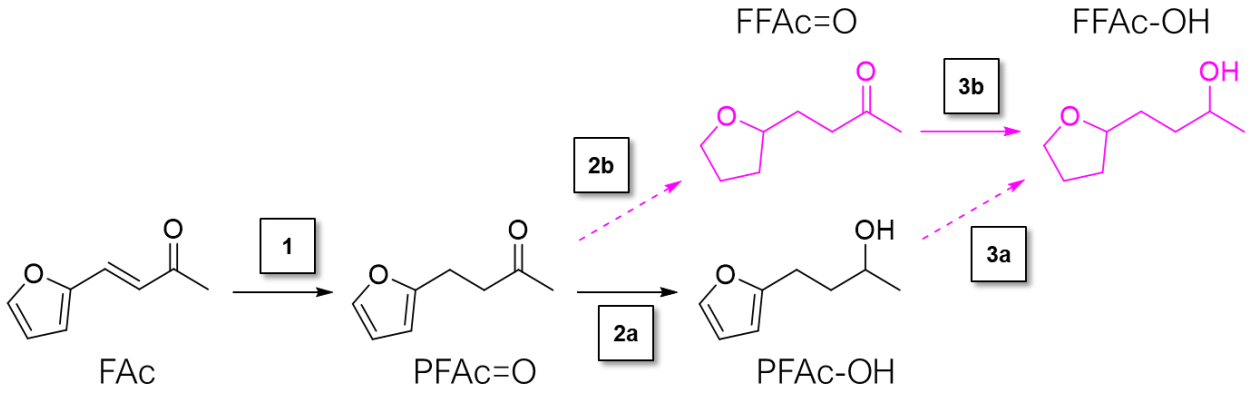

Scheme 1. Reaction network for FAc hydrogenation over Cu/γ-Al_2O_3. Black lines indicate the experimentally observed pathway, whereas pink lines denote possible furan ring hydrogenation pathways. Solid lines represent aliphatic double bond or carbonyl hydrogenation steps and dashed lines represent furan ring hydrogenation steps. PFAc stands for partially hydrogenated FAc. FFAc stands for fully hydrogenated FAc; Carbonyl and hydroxyl groups in PFAc are abbreviated to =O and -OH, respectively.

Table 1 shows the apparent activation energies (E_{app}) determined from our experiments on FAc hydrogenation over the Cu/γ-Al_2O_3 catalyst. The batch-calculated apparent activation energies for FAc hydrogenation agreed with reported values for batch HAH hydrogenation over Cu/γ-Al_2O_3.[7] The apparent activation energy barrier for batch hydrogenation of the aliphatic double bond of FAc (59 ± 29 kJ mol^{-1}) was 16 kJ mol^{-1} higher than hydrogenation of the first alkene group of HAH (43 ± 14 kJ mol^{-1}).[7] Moreover, the barrier for hydrogenation of the aliphatic double bond of FAc was similar to the hydrogenation barrier for the HAH double bond (58 ± 26 kJ mol^{-1}).[7] One possible explanation for the discrepancy between the aliphatic double bond hydrogenation barriers between HAH and FAc involves stronger dispersion interactions between HAH and its hydrogenated products with the Cu surface compared to FAc. The additional furan ring of HAH may stabilize surface adsorption, resulting in more facile hydrogenation of the first HAH alkene group. Further hydrogenation of the carbonyl group of PFAc=O and PHAH (PFAc=O analogue for HAH) proceeded with comparable barriers of ca. 40 kJ mol^{-1}. Despite minor discrepancies, the batch-calculated kinetic parameters for FAc hydrogenation were in close agreement with those determined for HAH.

Table 1. Apparent activation energies (E_{app}) calculated from fitting the reaction kinetics model to the experimental reaction kinetics data for the proposed steps of FAc hydrogenation (T = 313-393 K (40-120°C), P_{H2} = 55 bar, C_{FAc} = 56 mM in 2-propanol) over Cu/γ-Al_2O_3. Reaction steps are numbered according to Scheme 1. Values shown outside parenthesis are reported in units of eV, whereas values shown inside parentheses are reported in units of kJ mol^{-1}. Entries with "-" indicate a reaction that was not observed from GC-FID analysis. PFAc stands for partially hydrogenated FAc. FFAc stands for fully hydrogenated FAc; Carbonyl and hydroxyl groups in PFAc are abbreviated to =O and -OH, respectively.

		Apparent Activation Barrier, E_{app} [eV (kJ mol^{-1})]		
	Step	**FAc Continuous Flow**	**FAc Batch**	**HAH Batch[a]**
1	FAc → PFAc=O	0.58 ± 0.12 (56 ± 11)	0.61 ± 0.30 (59 ± 29)	0.45 ± 0.15 (43 ± 14)[b] 0.60 ± 0.27 (58 ± 26)[c]
2a	PFAc=O → PFAc-OH	0.43 ± 0.21 (42 ± 20)	0.37 ± 0.22 (35 ± 22)	0.42 ± 0.27 (41 ± 26)
2b	PFAc=O → FFAc=O	-	-	-
3a	PFAc-OH → FFAc-OH	-	-	-
3b	FFAc=O → FFAc-OH	-	-	-

[a]From Ref. [7]

[b]Hydrogenation of the first HAH aliphatic double bond

[c]Hydrogenation of the second HAH aliphatic double bond

2 Continuous Flow Experiments: Reaction Orders and Apparent Activation Energies

With FAc identified as a suitable surrogate molecule to model HAH hydrogenation, a more detailed reaction kinetics study was conducted for the Cu/γ-Al_2O_3 catalyst using a continuous flow reactor system, allowing for the equilibration of species adsorption and desorption on surface active sites at steady-state. This approach enables an assessment of intrinsic reaction kinetics without interference from mass transfer effects.[7] Flow experiments were performed under similar conditions to the batch reactions between 313-393 K (40-120°C). For all experiments, FAc was dissolved in 2-propanol and FAc conversion was maintained below 20% to measure turnover frequencies (TOFs). Reaction kinetics parameters were derived from steady-state concentrations according to the reaction scheme shown in Scheme 1. Concentration profiles from these continuous flow experiments are shown in Figure 3, with derived reaction kinetics parameters shown in Figure 4 and Table 1.

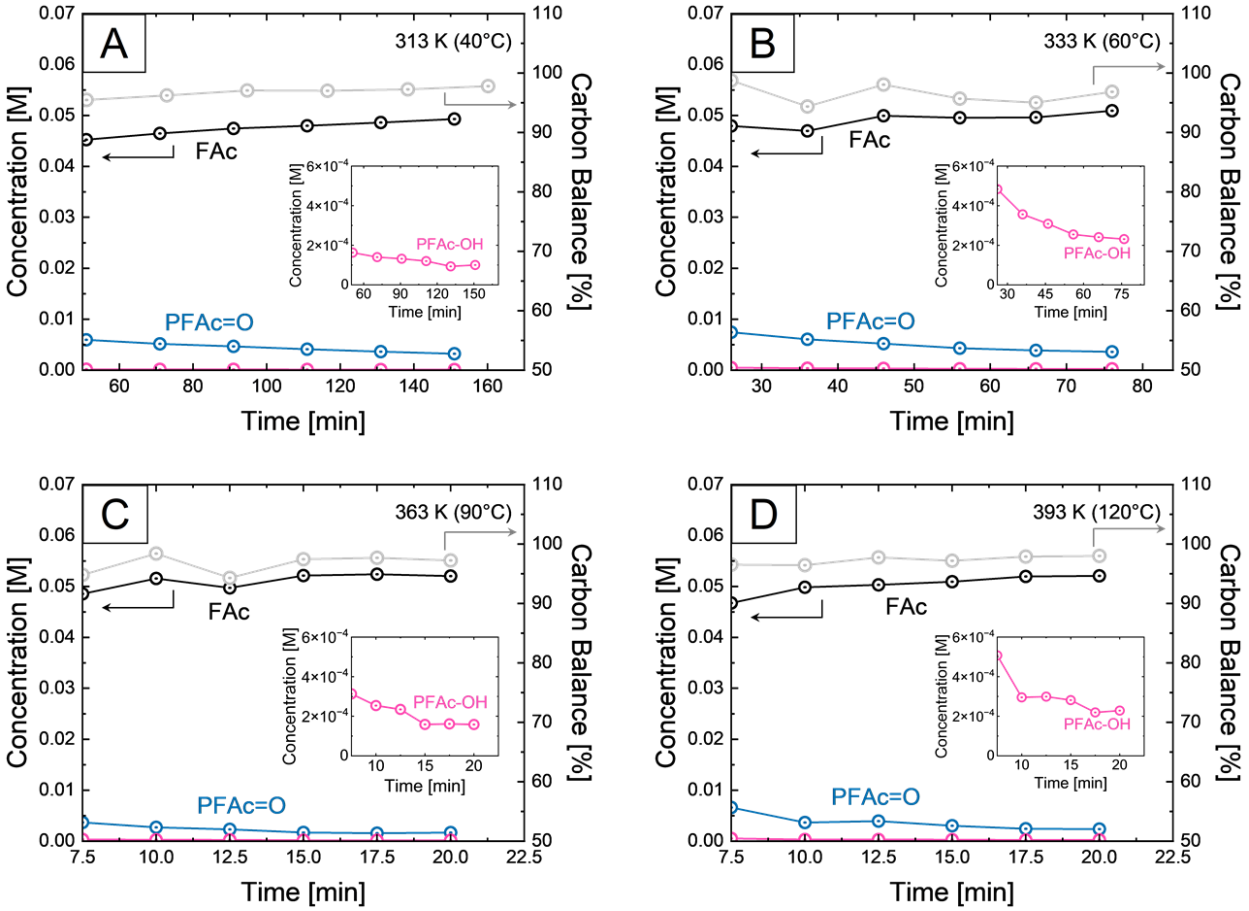

Figure 3. Concentration profiles for FAc hydrogenation over (A) 150 mg of 5 wt.% Cu/γ-Al_2O_3 at 313 K (40°C), (B) 65 mg of 5 wt.% Cu/γ-Al_2O_3 at 333 K (60°C), (C) 35 mg of 5 wt.% Cu/γ-Al_2O_3 at 363 K (90°C), and (D) 10 mg of 5 wt.% Cu/γ-Al_2O_3 at 393 K (120°C). Only data points after the initial product sample are shown. A gas H_2 flowrate of 25 mL min^{-1} was used along with a 56 mM FAc in 2-propanol liquid feed flowrate of (A) 0.25 mL min^{-1}, (B) 0.5 mL min^{-1}, or (C-D) 2.0 mL min^{-1}. PFAc stands for partially hydrogenated FAc; Carbonyl and hydroxyl groups in PFAc are abbreviated to =O and -OH, respectively.

From our continuous flow experiments, hydrogenation of the aliphatic double bond of FAc to produce PFAc=O proceeded with an activation energy of 0.58 ± 0.12 eV (56 ± 11 kJ mol^{-1}) (Figure 3(A)), which is comparable to the value of E_{app} derived from our batch FAc experiments and for batch HAH aliphatic double bond hydrogenation (Table 1).[7] Once formed, the PFAc=O carbonyl group hydrogenated to form PFAc-OH with an activation energy barrier of 0.43 ± 0.21 eV (42 ± 20 kJ mol^{-1}) (Figure 3(C)), the value of which is in agreement with the apparent activation barriers derived from batch FAc and HAH hydrogenation experiments.[7] As flow systems are more reliable for extracting reaction kinetics parameters, we focus the remainder of our discussion and theoretical studies on the results derived from continuous flow experiments.

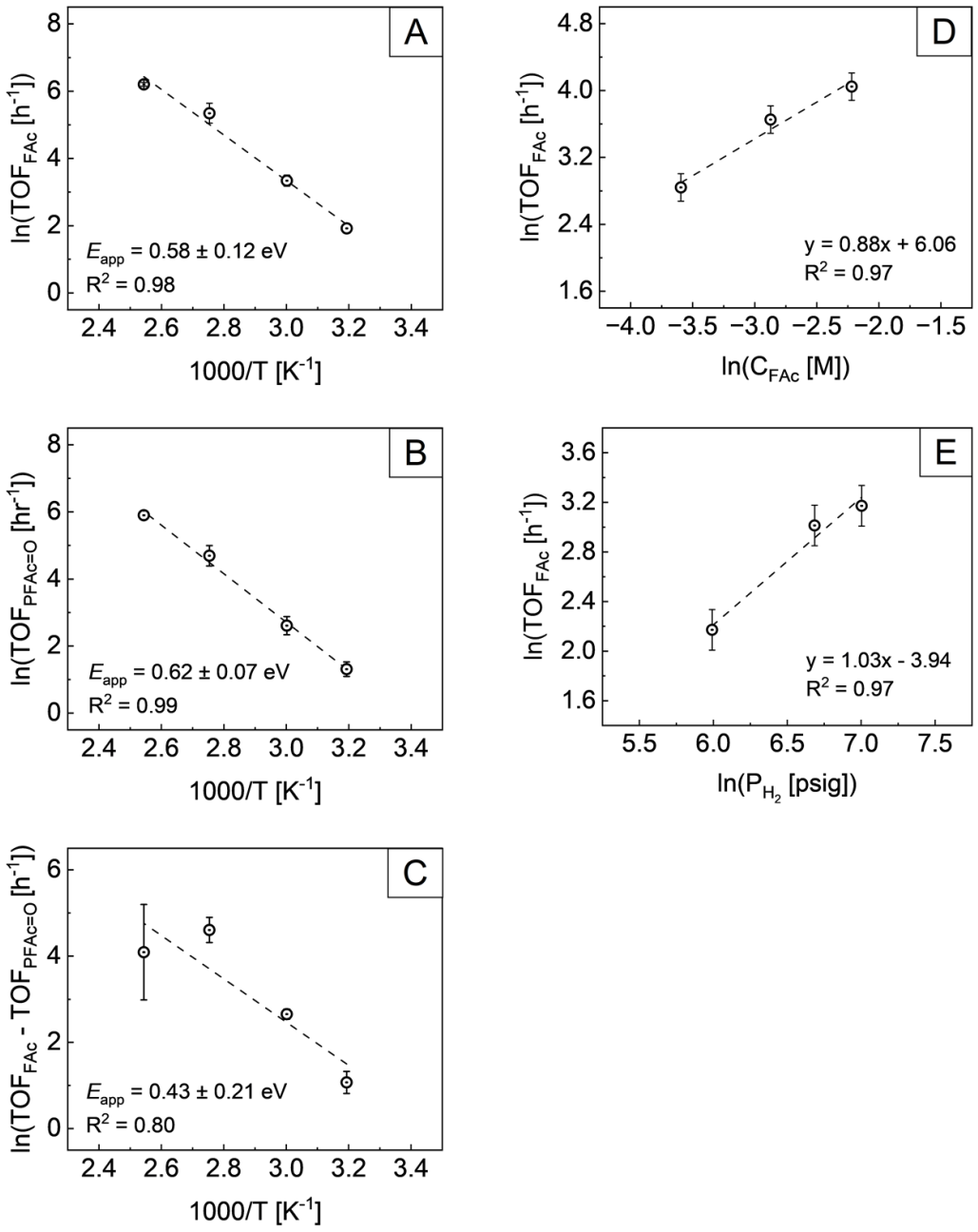

Figure 4. Arrhenius plots for FAc hydrogenation turnover frequencies (TOFs) from reaction kinetics modeling over 5 wt.% Cu/γ-Al_2O_3 for (A) a lumped consumption rate of FAc, (B) a lumped production/consumption rate of PFAc=O, and (C) the consumption rate of PFAc=O to produce PFAc-OH (step 2a in Scheme 1 of the main text). The temperature was varied between 313–393 K. An initial concentration of 56 mM FAc 2-propanol was used. For all experiments, the reactor was heated to the reaction temperature and loaded with 55 bar H_2. Data points (black) and error bars represent the mean TOF and standard error obtained from a set of triplicate experiments, respectively. (D-E) The effect of FAc concentration and H_2 partial pressure on the FAc hydrogenation TOF. Reaction orders were calculated as a lumped order derived from the rate of FAc consumption. The H_2 partial pressure was varied between 28-76 bar (400-1100 psi) for a FAc concentration of 56 mM FA in 2-propoanol. The FAc concentration was varied from 2.7-10.9 mM at a H_2 partial pressure of 55 bar (800 psi). All experiments were performed at 333 K. Error bars (blue) represent expected standard errors calculated as the mean standard error from the set of triplicate experiments in (A) performed at 333 K.

The reaction orders for FAc and H_2 were determined by varying the concentration of FAc in 2-propanol and the H_2 partial pressure. Figure 4(D-E) shows FAc and H_2 orders of approximately one, indicating first-order dependence on the rate of FAc hydrogenation. These results agree with reaction orders derived for HAH hydrogenation over Cu/γ-Al_2O_3, which were reported as near unity under similar experimental conditions in batch systems.[7] Regarding product selectivity, furan ring hydrogenation of FAc to produce FFAc=O or FFAc-OH was not observed under our reaction conditions (Figure 3).[7]

In summary, we derived reaction kinetics parameters and reaction orders for FAc hydrogenation using a continuous flow reactor. Qualitatively, batch experiments indicate that FAc is an appropriate surrogate for modeling HAH hydrogenation kinetics over Cu/γ-Al_2O_3 catalysts, given a two-step consecutive hydrogenation scheme similar to HAH. Finally, close agreement between the batch-calculated apparent activation barriers for FAc and HAH hydrogenation further implies that FAc is appropriate for modeling the reactivity of HAH on Cu catalysts.

3 Density Functional Theory Calculations

DFT calculations (see Methods) were performed to model the hydrogenation of FAc over a Cu(111) surface. Cu(111) is the most stable Cu crystal facet and is expected to be the dominant facet present in our Cu/γ-Al_2O_3 catalyst used in our experiments.[13] To maintain computational feasibility, the studied hydrogenation network was primarily focused on FAc and hydrogenated products observed in our experiments (PFAc=O and PFAc-OH). Moreover, despite not being observed experimentally, we also considered furan hydrogenation steps for FAc and PFAc=O to elucidate the unique hydrogenation behavior observed over Cu, in which no hydrogenation of the furan ring occurs. In total, a series of 17 elementary reaction steps involving 11 FAc-derived surface intermediates and 4 gas-phase species (FAc, PFAc=O, PFAc-OH, and H_2) were considered.[14,15] Because these calculations were aimed only at highlighting differences in the kinetic barriers of competing hydrogenation reaction steps, adsorbate coverage was limited at the dilute limit with a single adsorbed species per surface unit cell (1/16 monolayers (ML) = 0.0625 ML).

We first considered the adsorption of FAc on Cu(111). Minimum energy adsorption modes for FAc, as well as for PFAc=O and PFAc-OH, are shown in Figure 5(A). In its most stable adsorption state, FAc binds to the Cu(111) through the carbonyl O atom (ΔG_{ads} = -0.27 eV at T = 333 K and P_{FAc} = 4.4 × 10^{-7} bar) and with the plane of its furan ring 2.75 Å above the nearest Cu surface

atom. A charge density difference plot in Figure 5(B) depicting the change in electron density following FAc adsorption to Cu(111) reveals minor perturbations in the electron density between the furan ring and Cu surface atoms. This behavior suggests that the furan ring has weak interactions with the Cu(111) surface. Indeed, using the same PBE-D3 exchange correlation functional, Liu *et al.* reported that furan-containing compounds such as furfural, bind weakly to Cu surfaces at 400 K (ΔG_{ads} = ca. -0.3 eV) compared to other transition metals such as Ni (ΔG_{ads} = ca. -1.2 eV), Ru (ΔG_{ads} = ca. -1.8 eV), Rh (ΔG_{ads} = ca. -1.6 eV), Pd (ΔG_{ads} = ca. -1.1 eV), and Pt (ΔG_{ads} = ca. -1.2 eV).[16] Over stronger binding surfaces with *d*-band centers closer to the Fermi level,[17] furan ring C-C bonds may rehybridize from sp^2 to sp^3.[18] Such rehybridization prompts the furan oxygen to move away from the metal surface, allowing for a nearly flat adsorption mode with furan carbon atoms closely interacting with metal surface sites.[18] As seen in Figure 5, this rehybridization is not observed on Cu(111). The strength of interaction between the furan ring and the metal surface has important ramifications on the ability of the surface to hydrogenate the furan ring. Regarding the adsorption of hydrogenated intermediates and products, PFAc=O and PFAc-OH bind in planar configurations to Cu(111), with the furan rings distanced 2.88 and 2.79 Å from Cu surface atoms, respectively. Carbonyl binding to the Cu surface is disrupted for PFAc=O and PFAc-OH, with adsorption dominated by dispersion interactions. The weak interaction of the OH group in PFAc-OH with the Cu(111) surface may rationalize why the furan hydroxymethyl group, lacking in the surrogate FAc molecule, does not affect the hydrogenation pathway of the latter when compared to that of HAH.

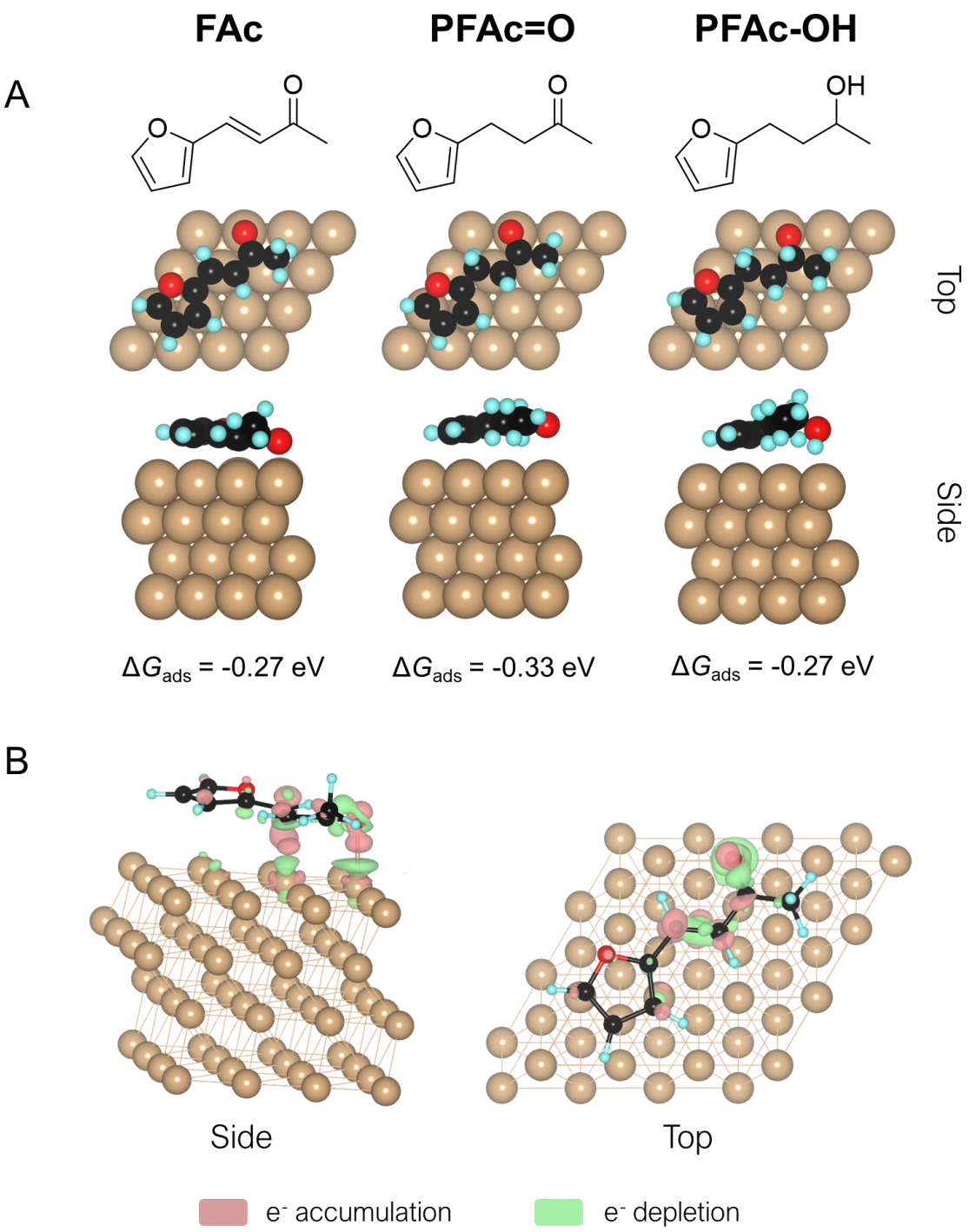

Figure 5. (A) Calculated minimum energy adsorption modes for 1/16 ML of FAc, PFAc=O, and PFAc-OH on pristine Cu(111). Adsorption free energies on Cu(111) (T = 333 K; P_{FAc} = 4.4 × 10^{-7} bar) are shown below slab side views. Top and side views of each slab are shown for each adsorbate. (B) Charge density difference plots showing side and top views for the change in electron density of FAc upon adsorption to Cu(111). Red isosurfaces represent regions of charge accumulation whereas green isosurfaces represent regions of charge depletion. Isosurfaces are plotted as 0.0025 $e^-/Å^3$. The following color scheme was adopted for the atoms shown: H - blue, C - black, O - red, and Cu - bronze.

While the adsorption modes shown in Figure 5(A) were calculated for pristine Cu(111), previous experimental studies have shown 0.5 ML saturation coverages for hydrogen adsorption on Cu(111),[19] Cu(100),[19] and Cu(110).[20,21] These coverages agree with our theoretical predictions for hydrogen coverage on Cu(111) under FAc hydrogenation conditions (Figure S5(A)). To assess the effects of hydrogen surface coverage, we further considered FAc, PFAc=O, and PFAc-OH binding to Cu(111) decorated with 0.5 ML H* in Figure S5(B). Similar to FAc adsorption on pristine Cu(111), FAc in its minimum energy adsorption mode remains bound atop the 0.5 ML H*-decorated Cu(111) surface through the carbonyl oxygen atom, with weak interactions between the furan ring and surface-bound hydrogen (Figure S6). The minimum energy adsorption modes of PFAc=O and PFAc-OH the 0.5 ML H*-decorated Cu(111) surface closely resemble those on the pristine Cu(111). Finally, the distance between the oxygen atom in the C=O group in FAc, PFAc=O, and PFAc-OH and the nearest Cu atom in the surface remains similar between the pristine and 0.5 ML H* coverage models, changing by between 0.09 and 0.16 Å for the two H* coverages (Table 2). Therefore, to a first approximation, we assume here that the minimum energy pathways for elementary FAc hydrogenation steps between the two coverage models are very similar. Accordingly, and for simplicity, we limit the following discussion to hydrogenation steps over the pristine Cu(111).

Table 2. Calculated CO-Cu bond lengths of FAc, PFAc=O, and PFAc-OH on pristine and 0.5 ML H*-decorated Cu(111). CO-Cu bond lengths are given by the distance of the closest Cu atom to the oxygen in the C=O group.

Species	C=O-Cu Bond Length [Å]	
	Pristine	0.5 ML H*
FAc	2.25	2.41
PFAc=O	3.18	3.34
PFAc-OH	3.17	3.08

Next, we considered the hydrogenation of FAc through the calculated Gibbs free energy surface shown in Figure 6 at T = 333 K (60°C), P_{H2} = 55 bar (800 psi), and P_{FAc} = 4.4 × 10^{-7} bar (6.4 × 10^{-6} psi), which represent the experimental HAH hydrogenation conditions. DFT-calculated activation energy barriers and reaction energies are overlayed on the reaction network shown in Scheme 2. Optimized structures of all initial states, transition states, and final states used to determine FAc hydrogenation barriers are shown in Supporting Information Figures S7-S9. The hydrogenation of the aliphatic double bond of FAc through its favored C4 carbon closest to the furan ring (black line) possesses a lower activation energy barrier (G_a = 0.57 eV for FAc* + H* → PFAc=O-int-C4*

+ *) than either furan ring hydrogenation (pink line; G_a = 0.66 eV; FAc* + H* → FAc-furan-int-C1* + *) or carbonyl hydrogenation (blue line; G_a = 0.58 eV; FAc* + H* → FAc-carbonyl-int-OH* + *). This result indicates that the aliphatic double bond of FAc and the carbonyl group are more likely to hydrogenate before the furan group. We note as a proxy for full hydrogenation of the furan ring, we limited our analysis to the addition of only the first hydrogen atom to the furan ring. Although additional reaction steps are required for full furan ring hydrogenation, we do not expect these additional steps to alter any conclusions over the Cu(111) surface. Over surfaces where furan ring hydrogenation is observed, such as Pd(111), the initial hydrogenation of furan rings in the α position to the ring oxygen (E_a = 1.22 eV; GGA-PBE-D3) , which closely resembles the geometry and bonding of our partially hydrogenated FAc species formed following TS-1 (FAc-furan-int-C1), was considerably more difficult than the second hydrogen addition step (E_a = 0.67 eV).[22]

Following the addition of the first hydrogen atom to the aliphatic double bond of FAc, addition of the second hydrogen atom to fully hydrogenate the aliphatic double bond and form PFAc=O is easier than the first H* addition (G_a = 0.27 eV for PFAc=O-int-C4* + H* → PFAc=O* + *). Regarding the competition between the aliphatic double bond (G_a = 0.57 eV for FAc* + H* → PFAc=O-int-C4* + *) and carbonyl (G_a = 0.58 eV for FAc* + H* → FAc-carbonyl-int-OH* + *) hydrogenation steps, we determined that carbonyl hydrogenation is significantly more endergonic (ΔG_{rxn} = 0.44 eV) than hydrogenation of the aliphatic double bond (ΔG_{rxn} = 0.27 eV for FAc* + H* → PFAc=O-int-C4* + *). Notably, the barrier associated with carbonyl hydrogenation of FAc (G_a = 0.58 eV) is similar to that for hydrogenation of the aliphatic double bond (G_a = 0.57 eV). However, further hydrogenation of FAc-carbonyl-int-OH (G_a = 0.39 eV for FAc-carbonyl-int-OH* + H* → FAc-carbonyl-OH* + *) possesses a larger kinetic barrier than the reverse step (G_a = 0.14 eV for FAc-carbonyl-int-OH* + * → FAc* + H*). Further, we also considered complete 1,4-hydrogenation of FAc, whereby an enol (PFAc-OH-C4) is formed in which the double bond is shifted to include the carbonyl carbon. The activation barriers for the 1,4-hydrogenation of FAc, proceeding through PFAc=O-int-C4 (G_a = 0.85 eV) or FAc-carbonyl-int-OH (G_a = 0.33 eV) were found to be significantly higher compared to the hydrogenation of PFAc=O-int-C4 to produce PFAc=O (G_a = 0.27 eV) or the dehydrogenation of FAc-carbonyl-int-OH to FAc (G_a = 0.14 eV). The 1,4-hydrogenation events discussed above are illustrated in Scheme 2 along with more detailed Gibbs free energy diagrams in Figure S10. Finally, we considered the keto-enol tautomerization of FAc-carbonyl-int-OH*, whereby the hydrogen on the carbonyl oxygen atom is transferred to neighboring carbon atoms in the aliphatic double bond. The activation barriers for these steps were also found to be prohibitively large (Figure S10). Although not directly

considered in this work, solvent-mediated mechanisms may facilitate keto-enol tautomerization steps.[23] Consequently, we expect the primary reaction flux to proceed through hydrogenation of the aliphatic double bond, which is consistent with our experimental observations.

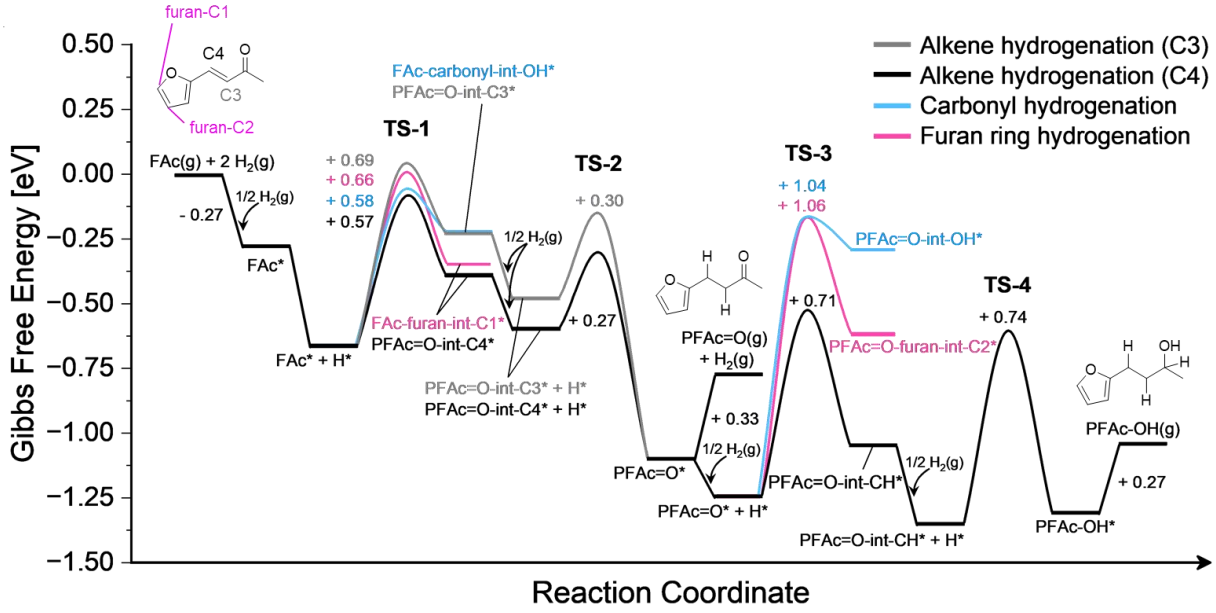

Figure 6. Calculated Gibbs free energy diagram (T = 333 K; P_{H2} = 55 bar; P_{FAc} = 4.4 × 10^{-7} bar) for FAc hydrogenation over a pristine Cu(111) surface. Black and gray lines denote the hydrogenation pathways proceeding first through hydrogenation of the aliphatic double bond of FAc (observed experimentally), whereas blue and pink lines denote alternative pathways resulting in carbonyl hydrogenation and furan ring hydrogenation (not observed experimentally), respectively. Barriers for select transition states (TS) are included along with schematics of chemical structures for gas-phase species. Asterisks (*) denote surface-bound species. PFAc stands for partially hydrogenated FAc; Carbonyl and hydroxyl groups in PFAc are abbreviated to =O and -OH, respectively. Species labeled with "-int-" in their name denote open-shell, surface-bound intermediate species.

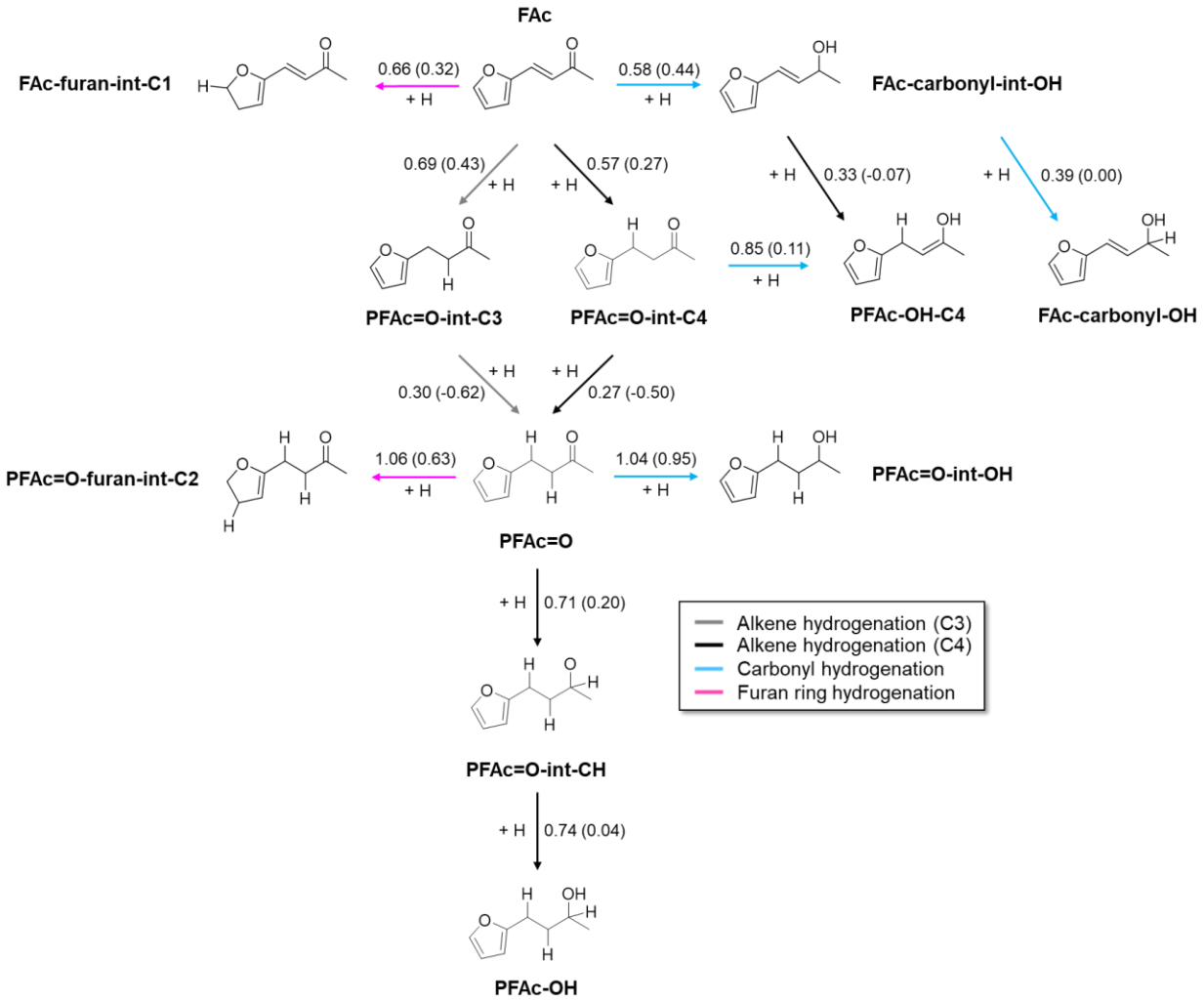

Scheme 2. Reaction network for the elementary FAc hydrogenation steps studied over pristine Cu(111). Calculated activation energy barriers and reaction energies under experimental reaction conditions (T = 333 K; P_{H2} = 55 bar; P_{FAc} = 4.4 × 10^{-7} bar) are shown above arrows. Values outside parentheses denote the calculated activation energy barrier (G_a) and values inside parentheses denote the calculated reaction energy (ΔG_{rxn}). All energies are reported in units of eV. Species labeled with "-int-" in their name denote open-shell, surface-bound intermediate species.

We next address the hydrogenation of PFAc=O. We find that the hydrogenation of the carbonyl group (G_a = 0.71 eV; PFAc=O* + H* → PFAc=O-int-CH* +) is slightly more difficult than previous hydrogenation steps for the aliphatic double bond (G_a = 0.57 eV for FAc* + H* → PFAc=O-int-C4* + *). Hydrogenation of the C=O bond through hydrogen addition to C and O atoms proceeds with activation energy barriers of 0.71 eV and 1.04 eV, respectively, implying that PFAc=O hydrogenation is likely to initiate through the carbonyl C atom (PFAc=O-int-CH). We again find that furan ring hydrogenation (G_a = 1.06 eV; PFAc=O* + H* → PFAc=O-furan-int-C2* + *) is more difficult than other PFAc=O hydrogenation steps. Finally, we note that desorption of adsorbed

PFAc=O (ΔG_{rxn} = 0.33 eV) is considerably easier than further hydrogenation of PFAc=O to produce PFAc-OH, suggesting that FAc hydrogenation largely terminates with the formation of PFAc=O under the studied reaction conditions. As discussed below, this is in agreement with our experimental findings.

Based on our DFT predictions, we find that the lowest energy pathway for conversion of FAc would involve the hydrogenation of FAc to form PFAc=O followed by PFAc-OH formation, which is consistent with the 2-step scheme we derived from batch reactor experiments. Additionally, our calculations indicate that furan ring hydrogenation is unfavorable over the Cu(111) surface. This prediction is consistent with experimental observations over Cu/γ-Al_2O_3, where no hydrogenation of the furan ring was observed. Our DFT results also predict more facile desorption of PFAc=O as opposed to further hydrogenation to PFAc-OH. This result agrees with experimental observations during our continuous flow experiments (Figure 3), in which the major species produced was PFAc=O, with low recorded steady-state PFAc-OH concentrations. In our high-conversion batch experiments (Figure 2), however, we observed complete hydrogenation to PFAc-OH. This result is expected given calculated barriers for PFAc=O hydrogenation to PFAc-OH of approximately 0.7 eV, which should be thermally accessible at the experimental reaction temperatures (313-393 K).

Using insights from our DFT calculations, we can understand the unique hydrogenation behavior of FAc/HAH over the Cu/γ-Al_2O_3 catalyst. Specifically, our DFT calculations suggest that weak interactions between the furan ring and Cu(111) are responsible for the lack of observed furan ring hydrogenation. From our continuous flow experiments, we derived an apparent activation energy of 0.58 ± 0.12 eV. In agreement, our DFT energetics indicate the largest activation energy barrier associated with FAc consumption was 0.57 eV. The highest calculated barrier for PFAc=O hydrogenation to form PFAc-OH (G_a = 0.74 eV for PFAc=O-int-CH* + H* → PFAc-OH* + *) was in modest agreement with the experimentally recorded activation energy barrier for PFAc-OH production of 0.43 ± 0.21 eV, with the discrepancy within the limit of DFT error.[24] A more detailed analysis of the reaction mechanism would require (i) explicit studies of the thermochemistry and kinetics of the hydrogenation steps discussed here as a function of surface coverages, including the H-decorated Cu(111) model discussed earlier, and (ii) considering different types of active sites, such as step edges, kinks, Cu-adclusters.[25]

Conclusions

We combined reaction kinetics experiments with DFT calculations to identify furfural acetone (FAc) as a suitable surrogate molecule for describing HMF-acetone-HMF (HAH) hydrogenation over a Cu catalyst. Through batch reaction kinetics experiments, we observed that FAc hydrogenation proceeds through a consecutive 2-step hydrogenation scheme similar to that of HAH hydrogenation, and that the furan ring does not undergo hydrogenation. Using a continuous flow reactor, we derived reaction kinetics parameters and reaction orders for FAc and H_2 (nearly one for both species). We observed that the hydrogenation of the aliphatic double bond and carbonyl group of FAc proceeded with apparent activation barriers of 0.58 eV and 0.43 eV, respectively, which are consistent with values obtained for HAH. With FAc identified as a suitable probe species for modeling HAH hydrogenation over Cu, we performed DFT calculations for the hydrogenation of FAc over Cu(111). Our computational predictions show that the hydrogenation of the aliphatic double bond of FAc is easier than furan ring hydrogenation. In agreement with the experimentally measured apparent activation barrier for PFAc=O production, we calculated a barrier for the first elementary hydrogenation step of the FAc aliphatic double bond of 0.57 eV. Further, desorption of partially hydrogenated carbonyl-containing FAc (PFAc=O) is energetically favored over continued hydrogenation of the carbonyl group, which explains the low yields of partially hydrogenated hydroxyl-containing FAc (PFAc-OH) obtained in our low-conversion continuous flow experiments. These insights may assist in the rational design of improved transition metal catalysts for the hydrogenation of complex organic compounds containing both aliphatic and aromatic double bonds.

Methods

Materials

Furfural acetone (98%, TCI America), 2-propanol (HPLC grade, Sigma-Aldrich), low soda gamma alumina (γ-Al_2O_3), 5 wt% Cu/γ-Al_2O_3 (Riogen), 18 MOhm Milli-Q water, H_2 (Industrial, Airgas), and Ar (Industrial, Airgas) were used as received. All batch reactions were carried out in a 45 mL Parr reactor (Parr Instrument Company) equipped with a dip tube for sampling during the reaction.

Catalyst Characterization

Pulse N_2O titration of the Cu/γ-Al_2O_3 catalyst was performed using a Micromeritics AutoChem 2920 at 365 K. N_2O consumption was monitored using a Cirrus 3 (Micromeritics) mass

spectrometer. A 2:1 stoichiometric ratio of Cu sites per N_2O molecule was assumed for estimating the number of active sites (91.9 μmol Cu/g_{cat}), the dispersion (11.7%), and the average particle diameter (8.9 nm) of the Cu/γ-Al_2O_3 catalyst.

Reaction Kinetic Studies over Cu Catalyst

Reactivity experiments were carried out in a 45 mL Parr batch reactor equipped with a dip tube for sampling. The Cu catalyst was reduced prior to the reaction at 573 K for 1 hour, with 3 K min^{-1} heating rates. A longer reduction for 5 hours at 573 K did not result in a significant difference in the obtained turnover frequencies. Reductions were performed by adding the catalyst to the batch reactor and purging with Ar to 30 bar twice and then purging with H_2 three times to 30 bar. The reactor was then filled with H_2 to 30 bar and heated to the reduction temperature at a rate of 3 K min^{-1}. Following reduction, the reactor was depressurized to slightly above atmospheric pressure. For all catalyst studies, 229 mg of furfural acetone (FAc) was dissolved in 30 mL of 2-propanol (56 mM) and fed into the Parr reactor using an HPLC pump. The reactor was then purged twice with 30 bar Ar and three times with 30 bar H_2. The reactor was then pressurized to 30 bar H_2 and heated to the desired reaction temperature at a heating rate of 3 K min^{-1}. The reactor was held at the reaction temperature and samples were taken with the dip tube. H_2 was replenished after sampling to maintain the reaction pressure. A pressure drop of 1-2 bar was observed after every two samples. Product samples were filtered with 0.2 μm polytetrafluoroethylene (PTFE) filters and analyzed by GC-FID. ^1H, ^{13}C, and HSQC NMR were implemented for samples that contained only one or two major products for the identification of molar ratios.

Reaction kinetics experiments in a continuous flow setup were also performed for 5 wt% Cu/γ-Al_2O_3 (Riogen) catalyst. A stainless-steel reactor with a 0.25-inch outer diameter (OD) operated in the fixed-bed up-flow configuration shown in Figure S4 was used. The catalyst was mixed with alpha alumina (STREM Chemical 99.5+%, mesh = 24-28) for a total mass of 500 mg. The catalyst mixture was immobilized by placing quartz wool on the top and bottom of the catalyst bed as well as a bed of silica chips (Sigma-Aldrich 99.9%, mesh 18-25). Reaction kinetics experiments were conducted with furfural acetone (FAc) diluted in 2-propanol (0.028 M - 0.1 M). The alpha alumina diluent and silica chips were chosen as they are inert for this reaction, and we find that no reaction occurs if we flow 1 M FAc in 2-propanol. The catalyst was reduced *in situ* at 573 K (300°C) in 100% H_2 for 1 hour (3 K min^{-1}) and cooled in H_2 to the reaction temperature. Similar conditions were used for reaction experiments performed in the batch reactors with reaction temperatures ranging from 313 K (40°C) to 393 K (120°C). The total pressure of 55 bar (800 psi) was used for

all experiments with a gas flow rate of 25 mL min^{-1}. The FAc in 2-propanol solution was controlled using an HPLC pump (Lab Alliance Series I) with a flow rate of 0.5 mL min^{-1} to 2.0 mL min^{-1}.

GC-FID Analysis of Hydrogenated Products

A gas chromatography (GC, Shimadzu GC-2010) equipped with a flame-ionizing detector (FID) and a Zebron ZB-50 column (ZB Inferno, Phenomenex, part no. 7HG-G00411) was used to quantify monomer species. All samples were filtered with 0.2 μm PTFE syringe filters prior to injection into the GC-FID.

NMR Characterization of Monomers

Product mixtures were collected from the Parr reactor, filtered with 0.2 um PTFE filters, and the solvent was evaporated. ^{1}H and ^{13}C nuclear magnetic resonance (NMR) spectra were obtained using a Bruker Avance-500 spectrometer. ^{1}H spectra (Figures S1-S3) were referenced to tetramethylsilane (TMS) at δ = 0 ppm and all other spectra used absolute referencing.

Reaction Kinetics Model

A reaction kinetics model was used to extract the reaction rate constants for each kinetic experiment. The reaction scheme illustrated in Scheme 1 detailing the sequential hydrogenation of FAc was used to generate the following rate equations:

$$r_{\mathrm{FAc}} = -k_1[\mathrm{FAc}] \quad (1)$$

$$r_{\mathrm{PFAc{=}O}} = k_1[\mathrm{FAc}] - k_2[\mathrm{PFAc{=}O}] \quad (2)$$

$$r_{\mathrm{PFAc{-}OH}} = k_2[\mathrm{PFAc{=}O}] \quad (3)$$

where $\boldsymbol{r_i}$ is the rate of consumption of species i, [i] is the concentration of species i, and k_i is the apparent rate constant for step i. The model was fitted to the experimental data by optimizing the rate constants using the non-linear least squares solver (lsqnonlin function) in MATLAB, and 90% confidence intervals were calculated using the nlparci function. Based on HAH hydrogenation results,[7] FAc hydrogenation was assumed to be first order with respect to H_2 partial pressure.

This pressure dependence is included in the rate constants as the reaction was held at a constant pressure of 55 bar H_2 for all kinetic studies in which kinetic modeling was performed. Steady-state concentrations were used for all kinetic parameter fitting and were taken as the average of three points for all flow reactions. A similar kinetic model was employed previously for HAH hydrogenation over transition metal catalysts.[7]

Density Functional Theory (DFT) Calculations

Density functional theory (DFT) calculations were performed using the PBE functional[14] with D3 dispersion corrections[15], as implemented in the Vienna *Ab initio* Simulation Package (VASP).[26,27] Plane waves were expanded to 400 eV and core electrons were approximated using projector-augmented wave (PAW)[28,29] potentials. Structures were converged until total energies were within 10^{-6} eV and forces were below 0.02 eV/Å. The Cu lattice constant was calculated to be 3.564 Å, which is in good agreement with the experimentally reported lattice constant of 3.615 Å.[30] The Cu(111) surface was modeled using a (4×4) slab comprised of four layers, in which the bottom two layers were fixed at their bulk lattice spacing. The electrostatic potential was adjusted to account for adsorption on only one side of the metal slab.[31,32] A vacuum layer of 20 Å was used to separate periodic images. A (6×6×1) Monkhorst-Pack *k*-point mesh[33] was used for all calculations. All structures were visualized using VESTA.[34]

Adsorption energies (ΔE_{ads}) were calculated as,

$$\Delta E_{\mathrm{ads,i}} = E_{\mathrm{i}} - E_{\mathrm{Cu(111)}} - E_i^{\mathrm{gas}} \quad (4)$$

where $\Delta E_{\mathrm{ads,i}}$ is the adsorption energy of species i, E_{i} is the electronic energy of the Cu(111) slab with adsorbed species i, $E_{\mathrm{Cu(111)}}$ is the electronic energy of the pristine Cu(111) slab, and E_i^{gas} is the electronic energy of species i in the gas phase. Similarly, adsorption free energies ($\Delta G_{\mathrm{ads,}}$) were calculated using Equation 5,

$$\Delta G_{\mathrm{ads,i}} = E_{\mathrm{ads,i}} + \Delta\mathrm{ZPE} + \int_0^T C_{P,i}\,dT - T\Delta S^{\circ} + RT\ln(P_i/P^{\circ}) \quad (5)$$

where $\Delta G_{\mathrm{ads,i}}$ is the adsorption free energy of species i, $\Delta \mathrm{ZPE}$ is the zero-point energy correction, $C_{P,i}$ is the constant pressure heat capacity of species i, ΔS° is the entropic correction, and T is the reaction temperature, 333 K (60°C). P_i and P° are the partial pressures of species i at 333 K and 1 bar, respectively. The partial pressure of FAc was calculated for a 56 mM FAc feed solution containing 229 mg of FAc and 30 mL IPA assuming ideal solution behavior. The partial pressures of PFAc=O and PFAc-OH were assumed identical to that of FAc. The enthalpic and entropic contributions to gas-phase species were calculated under the three-dimensional ideal-gas approximation, while surface contributions were calculated under the harmonic oscillator approximation. Numerical differentiation of the mass-weighted Hessian matrix was performed using a second-order finite difference approach with an ionic displacement of 0.015 Å.

Transition states used to evaluate the activation energy barriers for FAc hydrogenation were determined using the climbing-image nudged elastic band (CI-NEB) method in combination with the dimer method developed by Henkelman and co-workers.[35,36] CI-NEB calculations included seven intermediate images between the initial and final reaction states. Transition state saddle points were verified through a vibrational analysis yielding a single imaginary frequency in the direction of the reaction coordinate. Activation energy barriers (E_{a} or G_{a} for electronic and Gibbs free energies, respectively) were calculated using Equations 6-7,

$$E_{\mathrm{a}} = E_{\mathrm{TS}} - E_{\mathrm{IS}} \tag{6}$$

$$G_{\mathrm{a}} = G_{\mathrm{TS}} - G_{\mathrm{IS}} \tag{7}$$

where E_{TS} (G_{TS}) is the electronic (Gibbs free) energy at the transition state (TS) and E_{IS} (G_{IS}) is the electronic (Gibbs free) energy of the initial state (IS).

Author Contributions

Michael Rebarchik and Evangelos Smith contributed conceptualization, data curation, formal analysis, methodology, electronic structure calculations, visualization, and writing; Manos Mavrikakis and James A. Dumesic contributed conceptualization, project administration, supervision, funding, and writing; Hochan Chang contributed data curation, formal analysis, methodology, visualization, and writing.

Conflicts of Interest

There are no conflicts of interest to declare.

Supporting Information

^{1}H and ^{13}C NMR Spectra; Continuous flow experiments; Density functional theory (DFT) calculations

Acknowledgments

This work has been supported by the U.S. Department of Energy (DOE) through the Office of Basic Energy Sciences (BES); Catalysis Science Program, grant number DE-FG02-05ER15731. This research used computational resources of the National Energy Research Scientific Computing Center, a DOE Office of Science User Facility supported by the Office of Science of the U.S. Department of Energy under Contract No. DE-AC02-05CH11231 using NERSC award BES-ERCAP0032205, of the Center for Nanoscale Materials (CNM) at Argonne National Laboratory under contract number DE-AC02-06CH11357, and of the UW–Madison Center for High Throughput Computing (CHTC). CHTC is supported by UW-Madison, the Advanced Computing Initiative, the Wisconsin Alumni Research Foundation, the Wisconsin Institutes for Discovery, and the National Science Foundation. The authors thank Professor Siddarth H. Krishna and Matthew D. Edgar for assisting with catalyst characterization.

References

(1) Kong, X.; Zhu, Y.; Fang, Z.; Kozinski, J. A.; Butler, I. S.; Xu, L.; Song, H.; Wei, X. Catalytic Conversion of 5-Hydroxymethylfurfural to Some Value-Added Derivatives. *Green Chemistry* **2018**, *20* (16), 3657–3682. https://doi.org/10.1039/C8GC00234G.

(2) Rosatella, A. A.; Simeonov, S. P.; Frade, R. F. M.; Afonso, C. A. M. 5-Hydroxymethylfurfural (HMF) as a Building Block Platform: Biological Properties, Synthesis and Synthetic Applications. *Green Chemistry* **2011**, *13* (4), 754. https://doi.org/10.1039/c0gc00401d.

(3) van Putten, R.-J.; van der Waal, J. C.; de Jong, E.; Rasrendra, C. B.; Heeres, H. J.; de Vries, J. G. Hydroxymethylfurfural, A Versatile Platform Chemical Made from Renewable Resources. *Chem Rev* **2013**, *113* (3), 1499–1597. https://doi.org/10.1021/cr300182k.

(4) Chang, H.; Motagamwala, A. H.; Huber, G. W.; Dumesic, J. A. Synthesis of Biomass-Derived Feedstocks for the Polymers and Fuels Industries from 5-

(Hydroxymethyl)Furfural (HMF) and Acetone. *Green Chemistry* **2019**, *21* (20), 5532–5540. https://doi.org/10.1039/C9GC01859J.

(5) Strohmann, M.; Bordet, A.; Vorholt, A. J.; Leitner, W. Tailor-Made Biofuel 2-Butyltetrahydrofuran from the Continuous Flow Hydrogenation and Deoxygenation of Furfuralacetone. *Green Chemistry* **2019**, *21* (23), 6299–6306. https://doi.org/10.1039/C9GC02555C.

(6) Chang, H.; Gilcher, E. B.; Huber, G. W.; Dumesic, J. A. Synthesis of Performance-Advantaged Polyurethanes and Polyesters from Biomass-Derived Monomers by Aldol-Condensation of 5-Hydroxymethyl Furfural and Hydrogenation. *Green Chemistry* **2021**, *23* (12), 4355–4364. https://doi.org/10.1039/D1GC00899D.

(7) Gilcher, E. B.; Chang, H.; Huber, G. W.; Dumesic, J. A. Controlled Hydrogenation of a Biomass-Derived Platform Chemical Formed by Aldol-Condensation of 5-Hydroxymethyl Furfural (HMF) and Acetone over Ru, Pd, and Cu Catalysts. *Green Chemistry* **2022**, *24* (5), 2146–2159. https://doi.org/10.1039/D1GC04650K.

(8) Limmer, D. T.; Willard, A. P.; Madden, P.; Chandler, D. Hydration of Metal Surfaces Can Be Dynamically Heterogeneous and Hydrophobic. *Proceedings of the National Academy of Sciences* **2013**, *110* (11), 4200–4205. https://doi.org/10.1073/pnas.1301596110.

(9) Huber, G. W.; Chheda, J. N.; Barrett, C. J.; Dumesic, J. A. Production of Liquid Alkanes by Aqueous-Phase Processing of Biomass-Derived Carbohydrates. *Science (1979)* **2005**, *308* (5727), 1446–1450. https://doi.org/10.1126/science.1111166.

(10) Faba, L.; Díaz, E.; Vega, A.; Ordóñez, S. Hydrodeoxygenation of Furfural-Acetone Condensation Adducts to Tridecane over Platinum Catalysts. *Catal Today* **2016**, *269*, 132–139. https://doi.org/10.1016/J.CATTOD.2015.09.055.

(11) Chang, H.; Bajaj, I.; Huber, G. W.; Maravelias, C. T.; Dumesic, J. A. Catalytic Strategy for Conversion of Fructose to Organic Dyes, Polymers, and Liquid Fuels. *Green Chemistry* **2020**, *22* (16), 5285–5295. https://doi.org/10.1039/D0GC01576H.

(12) Chang, H.; Kim, M. S.; Gilcher, E. B.; Huber, G. W.; Dumesic, J. A. Development of Sustainable Processes for Production of Monomers and a Pharmaceutical Ingredient from Lignocellulosic Biomass. *Cell Rep Phys Sci* **2024**, *5* (3), 101859. https://doi.org/10.1016/J.XCRP.2024.101859.

(13) Tran, R.; Xu, Z.; Radhakrishnan, B.; Winston, D.; Sun, W.; Persson, K. A.; Ong, S. P. Surface Energies of Elemental Crystals. *Sci Data* **2016**, *3* (1), 160080. https://doi.org/10.1038/sdata.2016.80.

(14) Perdew, J. P.; Burke, K.; Ernzerhof, M. Generalized Gradient Approximation Made Simple. *Phys Rev Lett* **1996**, *77* (18), 3865–3868. https://doi.org/10.1103/PhysRevLett.77.3865.

(15) Grimme, S.; Antony, J.; Ehrlich, S.; Krieg, H. A Consistent and Accurate *Ab Initio* Parametrization of Density Functional Dispersion Correction (DFT-D) for the 94 Elements H-Pu. *J Chem Phys* **2010**, *132* (15), 154104. https://doi.org/10.1063/1.3382344.

(16) Liu, S.; Govindarajan, N.; Chan, K. Understanding Activity Trends in Furfural Hydrogenation on Transition Metal Surfaces. *ACS Catal* **2022**, *12* (20), 12902–12910. https://doi.org/10.1021/acscatal.2c03822.

(17) Hammer, B.; Nørskov, J. K. Theoretical Surface Science and Catalysis—Calculations and Concepts. In *Advances in Catalysis*; Academic Press, 2000; Vol. 45, pp 71–129. https://doi.org/10.1016/S0360-0564(02)45013-4.

(18) Bradley, M. K.; Robinson, J.; Woodruff, D. P. The Structure and Bonding of Furan on Pd(111). *Surf Sci* **2010**, *604* (11–12), 920–925. https://doi.org/10.1016/j.susc.2010.02.021.

(19) Anger, G.; Winkler, A.; Rendulic, K. D. Adsorption and Desorption Kinetics in the Systems H2/Cu(111), H2/Cu(110) and H2/Cu(100). *Surf Sci* **1989**, *220* (1), 1–17. https://doi.org/10.1016/0039-6028(89)90459-7.

(20) Bischler, U.; Sandl, P.; Bertel, E.; Brunner, T.; Brenig, W. Sticking, Adsorption, and Absorption of Atomic H on Cu(110). *Phys Rev Lett* **1993**, *70* (23), 3603–3606. https://doi.org/10.1103/PhysRevLett.70.3603.

(21) Rieder, K. H.; Stocker, W. Hydrogen-Induced Subsurface Reconstruction of Cu(110). *Phys Rev Lett* **1986**, *57* (20), 2548–2551. https://doi.org/10.1103/PhysRevLett.57.2548.

(22) Wang, S.; Vorotnikov, V.; Vlachos, D. G. A DFT Study of Furan Hydrogenation and Ring Opening on Pd(111). *Green Chem.* **2014**, *16* (2), 736–747. https://doi.org/10.1039/C3GC41183D.

(23) De Vrieze, J. E.; Thybaut, J. W.; Saeys, M. Role of Keto–Enol Tautomerization in the Copper-Catalyzed Hydrogenation of Ketones. *ACS Catal* **2019**, *9* (5), 3831–3839. https://doi.org/10.1021/acscatal.9b00279.

(24) Nørskov, J. K.; Abild-Pedersen, F.; Studt, F.; Bligaard, T. Density Functional Theory in Surface Chemistry and Catalysis. *Proceedings of the National Academy of Sciences* **2011**, *108* (3), 937–943. https://doi.org/10.1073/pnas.1006652108.

(25) Xu, L.; Papanikolaou, K. G.; Lechner, B. A. J.; Je, L.; Somorjai, G. A.; Salmeron, M.; Mavrikakis, M. Formation of Active Sites on Transition Metals through Reaction-Driven Migration of Surface Atoms. *Science (1979)* **2023**, *380* (6640), 70–76. https://doi.org/10.1126/science.add0089.

(26) Kresse, G.; Furthmüller, J. Efficient Iterative Schemes for *Ab Initio* Total-Energy Calculations Using a Plane-Wave Basis Set. *Phys Rev B* **1996**, *54* (16), 11169–11186. https://doi.org/10.1103/PhysRevB.54.11169.

(27) Kresse, G.; Furthmüller, J. Efficiency of Ab-Initio Total Energy Calculations for Metals and Semiconductors Using a Plane-Wave Basis Set. *Comput Mater Sci* **1996**, *6* (1), 15–50. https://doi.org/10.1016/0927-0256(96)00008-0.

(28) Kresse, G.; Joubert, D. From Ultrasoft Pseudopotentials to the Projector Augmented-Wave Method. *Phys Rev B* **1999**, *59* (3), 1758–1775. https://doi.org/10.1103/PhysRevB.59.1758.

(29) Blöchl, P. E. Projector Augmented-Wave Method. *Phys Rev B* **1994**, *50* (24), 17953–17979. https://doi.org/10.1103/PhysRevB.50.17953.

(30) *CRC Handbook of Chemistry and Physics*, 105th edition.; Rumble, J. R., Ed.; CRC Press, 2024.

(31) Neugebauer, J.; Scheffler, M. Adsorbate-Substrate and Adsorbate-Adsorbate Interactions of Na and K Adlayers on Al(111). *Phys Rev B* **1992**, *46* (24), 16067–16080. https://doi.org/10.1103/PhysRevB.46.16067.

(32) Bengtsson, L. Dipole Correction for Surface Supercell Calculations. *Phys Rev B* **1999**, *59* (19), 12301–12304. https://doi.org/10.1103/PhysRevB.59.12301.

(33) Monkhorst, H. J.; Pack, J. D. Special Points for Brillouin-Zone Integrations. *Phys Rev B* **1976**, *13* (12), 5188–5192. https://doi.org/10.1103/PhysRevB.13.5188.

(34) Momma, K.; Izumi, F. *VESTA 3* for Three-Dimensional Visualization of Crystal, Volumetric and Morphology Data. *J Appl Crystallogr* **2011**, *44* (6), 1272–1276. https://doi.org/10.1107/S0021889811038970.

(35) Henkelman, G.; Jónsson, H. A Dimer Method for Finding Saddle Points on High Dimensional Potential Surfaces Using Only First Derivatives. *J Chem Phys* **1999**, *111* (15), 7010–7022. https://doi.org/10.1063/1.480097.

(36) Henkelman, G.; Jónsson, H. Improved Tangent Estimate in the Nudged Elastic Band Method for Finding Minimum Energy Paths and Saddle Points. *J Chem Phys* **2000**, *113* (22), 9978–9985. https://doi.org/10.1063/1.1323224.